Journal of Materials Chemistry B

ROYAL SOCIETY OF CHEMISTRY

PAPER

View Article Online
View Journal | View Issue

Cite this: *J. Mater. Chem. B*, 2020, **8**, 6925

Tuning hydrogel properties with sequence-defined, non-natural peptoid crosslinkers†

Logan D. Morton, Alexander Hillsley, Mariah J. Austin and Adrianne M. Rosales *

Received 12th March 2020,
Accepted 14th May 2020

DOI: 10.1039/d0tb00683a

rsc.li/materials-b

The native extracellular matrix (ECM) is composed of hierarchically structured biopolymers containing precise monomer sequences and chain shapes to yield bioactivity. Recapitulating this structure in synthetic hydrogels is of particular interest for tissue engineering and *in vitro* disease models to accurately mimic biological microenvironments. However, despite extensive research on hydrogels, it remains a challenge to recapitulate the hierarchical structure of native ECM with completely synthetic hydrogel platforms. Toward this end, this work presents a synthetic hydrogel system using commercially available poly(ethylene glycol) macromers with sequence-defined poly(*N*-substituted glycines) (peptoids) as crosslinkers. We demonstrate that bulk hydrogel mechanics, specifically as shear storage modulus, can be controlled by altering peptoid sequence and structure. Notably, the helical peptoid sequence investigated here increases the storage modulus of the resulting hydrogels with increasing helical content and chain length, in a fashion similar to helical peptide-crosslinked hydrogels. In addition, the resulting hydrogels are shown to be hydrolytically and enzymatically stable due to the *N*-substituted peptidomimetic backbone of the crosslinkers. We further demonstrate the potential utility of these peptoid-crosslinked hydrogels as a viable cell culture platform using seeded human dermal fibroblasts in comparison to peptide-crosslinked hydrogels as a control. Taken together, our system offers a strategy toward ECM mimics that replicate the hierarchy of biological matrices with completely synthetic, sequence-defined molecules.

Introduction

In the native extracellular matrix (ECM), biopolymers such as collagen are made up of a specific sequence of amino acids that gives rise to highly integrated biological signaling, mechanical, and structural properties. Altering protein or polypeptide monomer sequence, even at the level of a single amino acid, can have dramatic effects on biopolymer chain structure and therefore bulk matrix properties.[1,2] While this high complexity gives rise to biofunctionality, it is also desirable to decouple features of the native ECM to create tunable *in vitro* platforms, such as for disease models or cell culture scaffolds. Incorporation of peptides or proteins into synthetic matrices has long been one key route to achieving this goal;[3,4] for example, adhesive peptides confer cellular attachment to several types of synthetic matrices independent of mechanics.[5–8] In addition, more recent work with unstructured poly(ethylene glycol) (PEG) hydrogels has shown that integration of a small amount of self-assembling, fibrillar peptides leads to encapsulated cell morphologies more similar to those in native collagen.[9] In these cases, the sequence definition of the biomolecules provides an extra handle to tune matrix properties. Excitingly, an increasing number of researchers are borrowing nature's strategy to control properties with sequence using peptidomimetics or synthetic macromolecules as well.[10] Non-natural, sequence-defined molecules offer the potential to fine tune matrix properties with enhanced stability and bio-orthogonality, mimicking features of natural biopolymers in engineered ECM.

Although reports detailing sequence effects on synthetic hydrogel or polymer matrix properties are still emerging, a number of platforms have shown promise in biomaterials applications. For example, poly(lactic-*co*-glycolic acid) (PLGA) microparticles with an alternating sequence of lactic and glycolic acid monomers exhibited a more uniform hydrolytic degradation profile as compared to random PLGA microparticles, which translated into fewer acidic byproducts and a lower foreign-body reaction.[11] In another example, solid-phase synthesized β-peptides were engineered to self-assemble into a network of nanofibers, resulting in a stable hydrogel that supported neural cell culture.[12] This non-proteinogenic network was proteolytically stable enough to support neuroblast migration to the cortex of transgenic

McKetta Department of Chemical Engineering, University of Texas at Austin, Austin, TX, USA. E-mail: arosales@che.utexas.edu; Tel: +1 512-471-6300

† Electronic supplementary information (ESI) available. See DOI: 10.1039/d0tb00683a

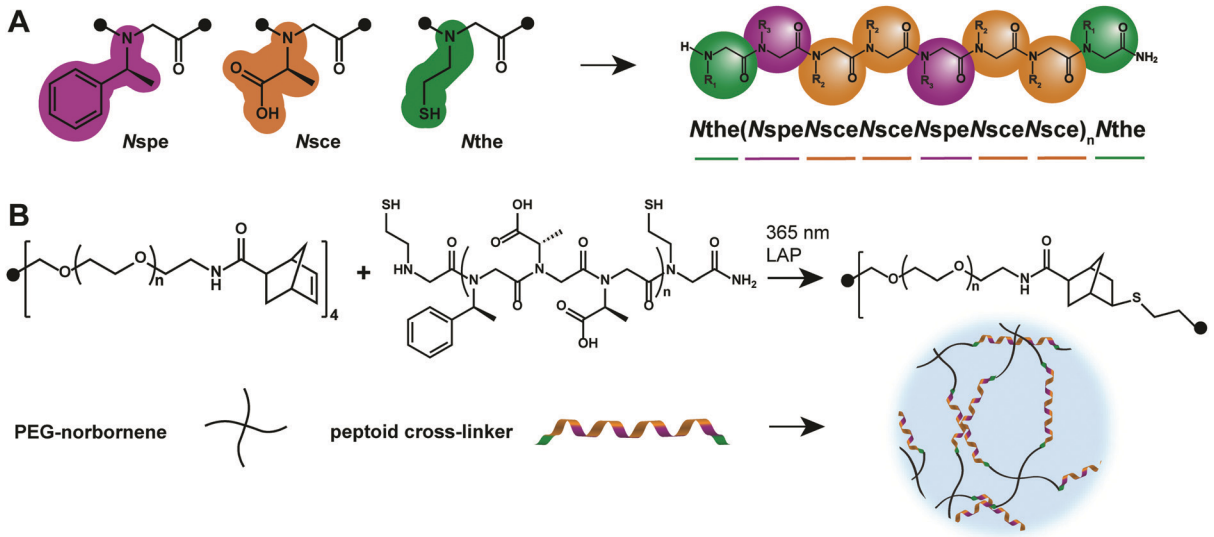

Fig. 1 (A) *N*-substituted glycine residues used in the helical peptoid crosslinkers. (B) Schematic representation of the photoinitiated thiol–ene crosslinking reaction between PEG-norbornene macromers and helical peptoid crosslinkers to form a hydrogel.

mice in a model of large brain injury.[13] Both of these systems leveraged the precise microstructures of non-natural backbones to influence bulk properties. As the synthesis of sequence-controlled and sequence-defined polymers continues to improve, it is anticipated that many more reports will add to these examples.

One such sequence-defined synthetic system of interest is peptoids, or *N*-substituted glycines (Fig. 1A). Peptoids are non-natural molecules that have been extensively investigated for their enhanced stability over peptides,[14] their suitability for either sequence-defined synthesis[15,16] or statistical polymerizations,[17–19] and their chemical diversity arising from primary amine submonomers. Furthermore, their specificity enables design of robust helical chain shapes[20,21] and protein-like structures.[22,23] In addition to their hierarchical structure, the reaction efficiency during chemical synthesis is high for many submonomers, leading to peptoid chain lengths that are well suited to the design of highly monodisperse hydrogel crosslinkers. In this regard, peptoid chemical diversity also enables facile incorporation of bio-orthogonal chemistries for crosslinking into the terminal side chains.

Given these features, we have investigated the use of peptoid-based crosslinkers in thiol–ene PEG hydrogels to control matrix properties (Fig. 1B). We first synthesized a series of helical peptoid oligomers with two thiol functionalities to react with norbornene-functionalized PEG macromers. Upon gelation, we demonstrated that the hydrogel properties were tunable with peptoid composition, length, and concentration, similar to other bi-functional crosslinkers. Interestingly, hydrogels crosslinked with helical peptoids increased in storage modulus as crosslinker length increased, demonstrating the impact of chain rigidity on bulk properties. Furthermore, we demonstrate that their non-natural backbone confers added stability in aqueous buffered solution, and in response to enzymatic challenge with collagenase and proteinase K. Finally, our work indicates that these hydrogels present a viable platform for cell culture applications, as indicated by the high viability of human dermal fibroblasts cultured on our matrix. We anticipate these results will further the development of sequence control as a strategy to finely tune biomaterial properties with synthetic macromolecules.

Experimental

Materials

4-Arm 10 kDa PEG–NH_2 was purchased from JenKem Technology USA (Plano, TX) at >95% amine substitution. Trt-Cysteamine·HCl (>99%), (*S*)-(−)-1-phenylethylamine (>99%), L-alanine-*tert* butyl ester (>97.5%), and Rink Amide Resin were all purchased from Chem-Impex International, Inc (Wood Dale, IL); α-methylbenzylamine (99%) was purchased from Sigma Aldrich (St. Louis, MO). All solvents were purchased from Fisher Scientific (Hampton, NH) and included the following: acetonitrile (>99.9%), dichloromethane (99.6%), diethyl ether (>95%), dimethylformamide (99.8%), and trifluoroacetic acid at (>95%). All reagents and solvents employed were commercially available and used as received without further purification. Proteinase K produced by the fungus *Tritirachium album* Limber was purchased from Promega Corporation (Madison, WI) and reported to have an activity of 41.0 units per mg. Gibco® Collagenase Type I isolated from *Clostridium histolyticum* was purchased from ThermoFisher Scientific (Waltham, MA) and reported to have an activity of 255 units per mg.

Peptoid synthesis

All peptoids (Table 1) were synthesized using Rink Amide polystyrene resin (0.43 mmol g^{-1} from Chem-Impex International, Inc.) on a Prelude X automated peptide synthesizer (Gyros Protein Technologies) at a scale of 250 μM according to previously published submonomer methods.[15,16] For each synthesis, fresh bromoacetylation reagent was made by dissolving 1.2 M bromoacetic acid in dimethylformamide (DMF). All displacement steps utilized 2 M primary amines in *N*-methyl-2-pyrrolidone (NMP), after freebasing

Table 1 Peptoid sequences for crosslinking based on *N*the(*N*spe*N*sce-*N*sce)$_n$*N*the

Sequence	n	N (total monomers)	M_{obs}/M_{theo}
1	2	8	1090.68/1090.23
2	4	14	1929.16/1929.10
3	6	20	2768.82/2767.97

when necessary. Once complete, all syntheses were cleaved from resin with 5 mL of 95 : 2.5 : 2.5 trifluoroacetic acid : water : triisopropylsilane for 4 hours. Prior to purification, the peptoids were dissolved at 10 mg mL^{-1} in 50 : 50 acetonitrile : water with 0.1% trifluoroacetic acid. The crude peptoids were purified with a C18 column on a Dionex UltiMate 3000 UHPLC using a 50 min gradient of acetonitrile in water (50–100%, 10 mL min^{-1}). After lyophilization, masses were verified *via* matrix-assisted laser desorption/ionization-time of flight (MALDI-TOF) mass spectrometry (Applied Biosystems – Voyager-DE™ PRO) and purity was confirmed *via* analytical HPLC (Fig. S1–S3, ESI†).

Peptide synthesis

Peptides were synthesized using Rink Amide polystyrene resin (0.72 mmol g^{-1} from Gyros Protein Technologies) on a Prelude X automated peptide synthesizer (Gyros Protein Technologies). Traditional Fmoc-mediated coupling methods were used at five-fold molar excess of amino acids and *O*-(1*H*-6-chlorobenzotriazole-1-yl)-1,1,3,3-tetramethyluronium hexafluorophosphate (HCTU) coupling reagent, and a ten-fold excess of *N*-methylmorpholine. Coupling steps were performed twice. Once complete, both syntheses were cleaved from resin with 10 mL of 95 : 2.5 : 2.5 trifluoroacetic acid : water : triisopropylsilane for 4 hours. Prior to purification, the peptides were dissolved at 10 mg mL^{-1} in 20 : 80 acetonitrile : water with 0.1% trifluoroacetic acid. The crude peptides were purified with a C18 column on a Dionex UltiMate 3000 UHPLC using a 25 min gradient of acetonitrile in water (20–100%, 10 mL min^{-1}). After lyophilization, masses were verified *via* MALDI-TOF (Fig. S4 and S5, ESI†). The sequences of the peptides synthesized are KCGGIQQWGPCK (for the peptide crosslinker control) and GCGYGRGDSPG (for cell adhesion).

Synthesis of norbornene-functionalized poly(ethylene glycol) (PEG-norbornene)

Multi-arm PEG-norbornene was synthesized by first activating 5-norbornene-2-carboxylic acid (0.244 mL, 2 mmol, 5.0 equiv.) with HBTU/HOBT (834.4 mg, 2.2 mmol, 5.5 equiv.) for 3 minutes in dimethylformamide (DMF, 1 mL) under an argon purge. *N*,*N*-Diisopropylethylamine (DIEA, 0.418 mL, 6.0 equiv.) was added to this activated solution and stirred for 5 minutes at room temperature. Next, this solution was added to an argon purged flask containing 4-arm, 10 kDa PEG-amine (1.0 g, 1.0 equiv.), and the reaction proceeded upon stirring for 24 h at room temperature. Upon completion of the reaction, the product was precipitated in cold ethyl ether (60 mL, 3×), and dialyzed for 3 days in distilled water before use. The product was recovered as a white solid. Yield = 93%, functionalization = 90% (Fig. S6, ESI†). ^{1}H NMR (D_2O, 400 MHz): δ 6.20 to 5.86 (m, 2H), δ 3.65 to 3.40 (m, 227H).

Hydrogel preparation

All gelation solutions were 50% acetonitrile and 50% phosphate buffered saline with 0.05 wt% lithium phenyl-2,4,6-trimethylbenzoylphosphinate (LAP) and 0.2 mM tris(2-carboxyethyl)-phosphine (TCEP). Unless otherwise stated, all hydrogels were 4-arm 10 wt% PEG-norbornene crosslinked at 1 : 1 thiol : ene ratio with peptide or peptoid at a concentration of 36 mM (72 mM thiol concentration) in 50 : 50 acetonitrile : water. Gelation was induced *via* exposure to 365 nm light (10 mW cm^{-2}, 1 min). For experiments with live cells, the hydrogels were functionalized with 2 mM RGD to allow for cell adhesion, and hydrogels were swollen overnight in PBS or media to remove the acetonitrile prior to cell seeding.

Rheometry

A Discovery HR-2 rheometer (TA Instruments) was used to perform all *in situ* gelation mechanics measurements. An 8 mm flat stainless steel geometry and a UV-transparent quartz plate were used for all experiments. Briefly, the macromer solution (15 μL) was pipetted onto the quartz plate, which was connected *via* liquid filled light guide to a mercury lamp (Omnicure Series 1500) fitted with a 365 nm filter. The macromer solution was exposed *in situ* to 365 nm light (10 mW cm^{-2}, 1 min) to cause gelation. Time sweeps were performed at 1 rad s^{-1} and 1% strain.

Circular dichroism (CD)

CD spectra were acquired from 180 to 280 nm using a Jasco J-815 CD Spectropolarimeter at 25 °C. Samples (200 μL) were prepared at 2 mM in 20% acetonitrile in water for each of the peptoids. A spectrum of pure 20% acetonitrile in water was subtracted from each sample spectrum to remove background. A quartz cuvette with a 1 mm path length was used for all samples. Mean residue ellipticity was calculated using the following equation:

$$[\theta] = m^\circ \times M/(10 \times L \times C \times n) \quad (1)$$

where m° is the CD given in millidegrees, M is the molecular weight (g mol^{-1}), L is the path length of the cell in cm, C is the concentration of peptoid in g L^{-1}, and n is the number of monomers.

Hydrogel stability

To assess hydrogel stability, hydrogels were made using 34 μL of macromer solution between two hydrophobically treated glass slides fitted with a silicon spacer (0.5 mm thick). After gelation, hydrogels were transferred to 12 well plates where they were allowed to swell in PBS overnight at 37 °C. After this swelling period, the PBS was replaced with 1 mL of degradation buffer. For collagenase, the degradation buffer consisted of 255 units per mg collagenase at 20 μg mL^{-1} in buffer containing 50 mM tricine, 10 mM calcium chloride, and 400 mM sodium chloride. For proteinase K, the buffer consisted of 20 μg mL^{-1} proteinase K with the additions of 50 mM Tris–HCl and 10 mM calcium chloride. PBS alone was used as a control. The buffers

were replaced at each time point with fresh solutions, and the removed volume was tested for mass loss *via* a NanoDrop OneC Microvolume UV-Vis Spectrophotometer at 205 nm employing the Protein A205 method in Scopes mode and comparing to a standard calibration curve confirmed to be linear between 0.01–10 mg mL^{-1}.

Cell viability

An MTT assay was used to measure cellular metabolic activity as an indicator of cell viability for human dermal fibroblasts (Lonza) seeded on the hydrogels or directly onto a Nunclon Delta Surface clear 96 well plate (Thermo Scientific) as a control. All hydrogels were photo-crosslinked at the bottom of the plate with 75 μL of macromer solution. After light exposure (365 nm, 10 mW cm^{-2}, 1 min), the hydrogels were washed 3 times with phosphate buffered saline (PBS) and allowed to incubate in PBS overnight at 37 °C. The following day, the PBS was replaced with Dulbecco's Modification of Eagle's Media (DMEM) (+10% Fetal Bovine Serum (Corning) +1% Penicillin–Streptomycin (Fisher Scientific)), and the hydrogels were allowed to incubate for another 2 hours before human dermal fibroblasts were seeded onto the hydrogels at 5200 cells per cm^2. The cells were cultured on the hydrogels for 1 day at 37 °C and 5% CO_2. Metabolic activity was measured using a Vybrant MTT kit (Thermofisher). Briefly, 10 μL of 3-(4,5-dimethylthiazol-2-yl)-2,5-diphenyltetrazolium bromide (MTT) was added along with 100 μL of serum-free media and allowed to incubate for 4 hours. Sodium dodecyl sulfate (SDS) was subsequently added and incubated for another 4 hours to lyse the cells and solubilize the metabolized MTT. Once complete, the absorbance from all wells was measured using a Synergy H1 Hybrid Multi-Mode Reader at a wavelength of 570 nm.

Live/dead assay and fluorescence microscopy

To further quantify the human dermal fibroblast viability on the hydrogels, a live/dead membrane integrity assay (LIVE/DEAD Viability/Cytotoxicity kit, for mammalian cells-Invitrogen) was performed. First, both peptoid and peptide-crosslinked hydrogels (5 wt%, 1 : 1 thiol : ene ratio) were made between a thiol-functionalized glass coverslip and a hydrophobically treated glass slide. The slide was separated from the coverslip, and the hydrogel-functionalized coverslip was placed in a low adhesion 12 well tissue culture plate with 1 mL PBS. The hydrogels were then washed 3 times with PBS and left to swell in PBS at 37 °C overnight. The PBS was subsequently replaced by media, allowed to swell for another 2 hours, and subsequently seeded with human dermal fibroblasts at a density of 5200 cells cm^{-2} in media. The cells were allowed to adhere and grow for 48 hours before application of 1 μM calcein-AM and 4 μM ethidium homodimer-1 for 30 min. Cells were imaged on a Nikon Eclipse Ti2 microscope. Cells in which the membrane-permeable calcein-AM was cleaved were counted as live, while cells permeable to ethidium homodimer were counted as dead. Cell area was also measured for all hydrogels that were imaged by converting them to binary images and measuring using FIJI's built in Analyze Particles feature. Over 40 cells were counted per hydrogel, and for each condition, 3 hydrogels were measured. Error bars represent standard deviation.

Statistics

Two-sample *t*-tests were completed for all data that is directly compared to determine if the means were statistically different, and one-way ANOVA tests were run on any trends with more than two data sets. In both cases, $p < 0.05$ was used as the cutoff for statistical significance.

Results and discussion

Development of peptoid crosslinked hydrogels

Previous strategies for synthesis of peptoid-based hydrogels have relied on non-covalent interactions, such as low molecular weight gelator assembly (similar to peptides)[24,25] or gel–sol transitions of triblock copolypeptoids synthesized by ring-opening polymerization.[26] These studies have indicated tunability in hydrogel properties with peptoid composition and concentration, as well as kinetic effects due to temperature or solvent changes during gelation. Importantly, these studies have also indicated minimal cytotoxicity, in line with peptoid work on other biomaterial platforms.[27] As a complementary strategy to these efforts, we sought to leverage the stability and biocompatibility of the peptoid backbone with the precise microstructure of solid phase synthesized peptoids to tune hydrogel properties. Due to the stepwise submonomer synthesis method, monodisperse sequences and chain lengths can be synthesized, as indicated by MALDI (Fig. 2A) and analytical HPLC (Fig. 2B). We reasoned that combining this monodispersity and an idealized network structure would enable investigation of peptoid crosslinker parameters on hydrogel properties in a fashion similar to covalently-linked hydrogels with peptide crosslinkers.

To select appropriate peptoid crosslinkers, we first identified a hydrophilic, chiral peptoid sequence known to form helices from previously published research (Fig. 1A).[28] Peptoid helices have a greater persistence length than non-helical peptoids,[29,30] which we hypothesized may be beneficial for presentation of reactive groups for hydrogel crosslinking in solution. In addition, the helical sequences offer a potential route to controlling bulk hydrogel mechanics.[31,32] Thus, to probe this hypothesis, we focused on a sequence with a repeating trimer motif of $(N\text{spe}N\text{sce}N\text{sce})_n$, where the *N*spe contained a bulky chiral aromatic as a steric driver of conformation and *N*sce contained a chiral carboxylic acid side chain to improve water solubility. Three different chain lengths containing this motif in which n = 2, 4, or 6 were successfully synthesized, as indicated by mass spectrometry (sequences **1–3**, Table 1). Furthermore, we synthesized a peptide sequence (KCGGIQQWGPCK) as a control, as these molecules have been used extensively as crosslinkers in step-growth PEG hydrogels in literature.[33–36] The selected peptide sequence contained a random internal sequence of amino acids to avoid secondary structure, and MALDI indicated successful synthesis with an

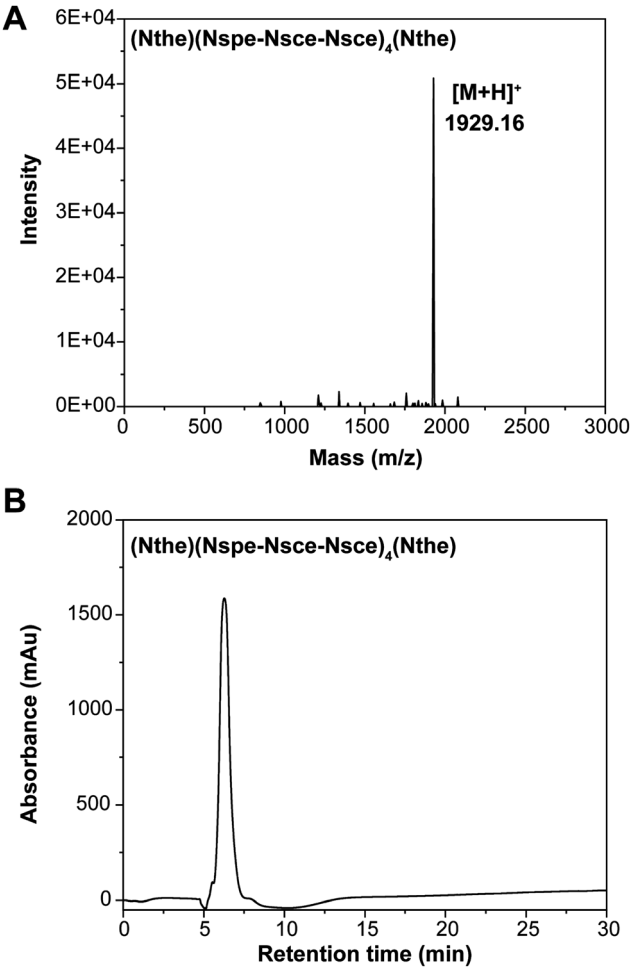

Fig. 2 (A) Representative MALDI confirming successful synthesis of sequence **2** (M_{obs}/M_{theo}): 1929.16/1929.10. (B) Representative HPLC trace confirming high purity of sequence **2** in excess of 95%.

observed mass-to-charge ratio (m/z) of 1303 compared to an expected m/z of 1303.6.

To generate peptoid-crosslinked hydrogels, we utilized photo-initiated thiol–ene chemistry (Fig. 1B). As previously mentioned, this route has been extensively used with peptide-crosslinked hydrogels, in part due to its high kinetic tunability, spatiotemporal control, and ease of incorporation using native amino acids in peptides (*e.g.*, cysteine).[37,38] Thus, sequences **1–3** were synthesized with *N*the moieties at the terminal residues to add reactive thiol groups and allow them to be used as crosslinking agents. Similarly, the peptide control contained two terminal cysteine residues for crosslinking. For the synthesized peptoid crosslinkers, tests using Ellman's reagent confirmed high availability of free thiols for further reaction (Fig. S7, ESI†).

To generate idealized network structures, 4-arm, 10 kDa poly(ethylene glycol)-amine was functionalized with norbornene groups in high yield (90%) and used as the macromer for all hydrogels in subsequent experiments. The two precursors were mixed at the desired concentration in a mixture of acetonitrile and water, and gelation was achieved using LAP photoinitiator and 365 nm light (10 mW cm^{-2}, 1 min). The reaction occurred rapidly, and 95% of the final plateau storage modulus was achieved within 30 seconds (Fig. 3A) of photoinitiation.

The peptoid crosslinked hydrogels exhibited highly tunable mechanics. As is typical of covalently crosslinked hydrogels, these constructs showed largely elastic behavior as indicated by the relatively small loss modulus (Fig. S8, ESI†). Furthermore, the ability to control the hydrogel storage modulus was demonstrated by altering the polymer concentration (Fig. 3B). For hydrogels crosslinked with sequence **2**, an increase in the polymer concentration from 5 wt% to 10 wt% led to a corresponding increase in hydrogel storage modulus from approximately 1800 Pa to 4700 Pa, due to the higher crosslinking density.

Notably, the greatest storage modulus was observed when the peptoid crosslinker was added in a 1 : 1 thiol : ene ratio, indicating near quantitative functionalization of the peptoids and PEG-norbornene macromers (Fig. 3C). For lower thiol : ene ratios (*i.e.*, 0.75 : 1 thiol : ene) in a 5 wt% hydrogel crosslinked with sequence **2**, the storage modulus dropped significantly to less than 100 Pa. While decreasing the number of thiol groups present is expected to decrease the number of elastically active crosslinks, this especially large drop in modulus suggests this 5 wt% formulation is close to the critical crosslinking density. Indeed, calculation of this threshold by Flory–Stockmayer

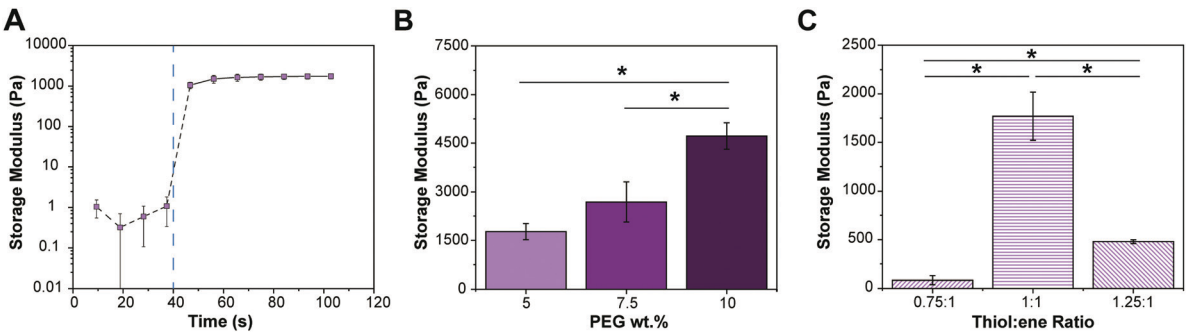

Fig. 3 (A) *In situ* gelation of a 5 wt%, 1 : 1 thiol : ene peptoid-crosslinked hydrogel. Blue dashed line indicates light initiation. (B) Storage modulus of 1 : 1 thiol : ene PEG hydrogels crosslinked with sequence **2** for various polymer concentrations. (C) Storage modulus of 5 wt% PEG hydrogels crosslinked with sequence **2** varying the ratio of thiol : ene.

gelation theory at this thiol : ene ratio is 0.96 on a per mole basis, meaning that 96% of the functionalities must react to form a hydrogel (see ESI†). Small fluctuations around this threshold may lead to dramatic effects in the observed storage modulus. For higher thiol : ene ratios (*e.g.*, 1.25 : 1 thiol : ene), increasing the number of thiol groups likewise decreases the storage modulus by oversaturating the norbornene groups, making it less likely for a single crosslinker to react with two different norbornene functionalities and create an elastically effective linkage. Thus, for the most uniform and ideal hydrogel network, a 1 : 1 thiol : ene ratio was used for all subsequent studies.

Impact of peptoid crosslinker structure on hydrogel mechanics

In addition to polymer concentration and thiol : ene ratio, crosslinker length was also varied as an alternative strategy to tune hydrogel mechanics (Fig. 4A). Sequences **1**, **2**, and **3** contained 8, 14, and 20 residues, respectively. Each of these sequences was incorporated at a 1 : 1 thiol : ene ratio in a 5 wt% hydrogel. Interestingly, the longer peptoid sequences increased the storage modulus of the hydrogel in direct contradiction of the trend predicted by rubber elasticity theory. Hydrogels crosslinked with sequence **3** exhibited a plateau modulus of 2700 Pa, which was approximately 2.25 times higher than that of hydrogels crosslinked with sequence **1**, which was 1200 Pa. Each addition of the hexameric repeat motif to the peptoid sequence contributed an increase of 1.5 times the storage modulus. These results indicated that increasing peptoid helix length led to an increase in chain rigidity over this range of sequence lengths.

To probe the helical conformation of the peptoid crosslinkers, we analyzed their absorption behavior by circular dichroism in a mixture of acetonitrile and water (Fig. 4B). Helical conformation was indicated by signature circular dichroic spectra containing negative peaks at 220 and 200 nm as well as a positive peak at 190 nm, matching the previously published spectrum for the same sequence with a similar per residue molar ellipticity in the range of -10^4 to 10^4.[28] Although the solvents used here differ from that previous study, the secondary structure of this sequence was shown to have little dependence on environmental conditions, unlike polypeptide α-helices, indicating that helicity was maintained in the studies discussed here. Previous reports also indicated that longer chiral peptoid sequences form more robust helices.[20,21] Indeed, circular dichroism demonstrated an increase in the per residue molar ellipticity for sequences **2** and **3** as compared to sequence **1** (Fig. 4B). It is anticipated that the more robust helices may exhibit increased chain stiffnesses (*i.e.*, higher persistence length), thereby imparting greater mechanical properties to the hydrogels. Previous work indicated a similar, though more marked, effect of persistence length when polypeptide α-helices were used as crosslinkers in PEG hydrogels.[31] Unlike peptide helices, which are stabilized by hydrogen bonds, the peptoid helical conformations here were induced *via* steric interactions, which may still impart considerable conformational flexibility to the chains. This may be one reason why the peptoid

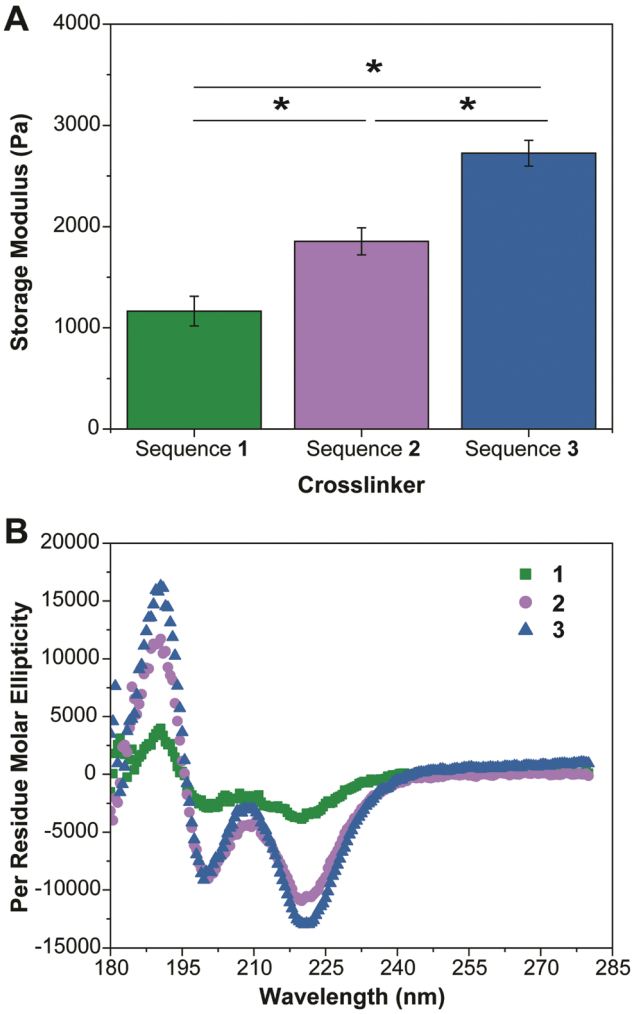

Fig. 4 (A) Increased crosslinker length increases the storage modulus of 5 wt% hydrogels crosslinked with sequences **1**, **2**, and **3**. (B) Circular dichroism comparing the secondary structures of sequences **1**, **2**, and **3**, indicating helical conformations for all, and higher per residue molar ellipticity with increased chain length.

crosslinkers led to a smaller increase in storage modulus with increasing helical content, as compared to that seen in peptide-based systems. Taken together, these data indicate that chain shape offers an alternate route to modulate hydrogel stiffness independent of network connectivity. We anticipate that the large chemical diversity of peptoids will enable further tunability of chain stiffness effects,[39–41] allowing for precise decoupling of matrix modulus and network connectivity, which may have applications for cell culture matrices that investigate the impact of mechanics on cellular phenotype.[42]

Peptoid hydrogel stability

Toward cell culture applications, one unique feature of peptoid-crosslinked hydrogels is their enhanced stability when compared to hydrogels crosslinked with peptides or other naturally derived counterparts. To investigate the stability of these linkages, both peptoid and peptide-crosslinked hydrogels were formed using silicon spacers to ensure uniform hydrogel size. Peptide hydrogels

were formed between two hydrophobically treated slides, while peptoid hydrogels were formed on a silicon base due to the wetting properties of the acetonitrile/water mixtures. These hydrogels were swollen overnight in PBS at 37 °C to reach an equilibrium state prior to exposure to one of three degradation conditions. Both the peptide-crosslinked and the peptoid-crosslinked hydrogels swelled to a similar extent (Fig. S9, ESI†). The degradation conditions were buffer alone, 20 μg mL^{-1} collagenase, or 20 μg mL^{-1} proteinase K. Both collagenase and proteinase K are broad spectrum proteases that are relevant to cell culture applications. Collagenase mimics the cell secreted proteases that direct matrix remodeling during homeostasis, wound healing and disease. Proteinase K is commonly used in molecular biology assays to digest nucleases and other contaminants during nucleic acid preparation. Stability to both proteases could enhance cell culture applications, particularly for 2D configurations where a stable hydrogel is desirable or in cases where long term stability of the scaffold is required *in vivo*.

Upon exposure to degradation conditions, aliquots were taken for each hydrogel condition at 1, 3, 5, 24, 48, and 72 hours and monitored for released peptide or peptoid chains *via* absorbance at 205 nm. All hydrogels were found to be hydrolytically stable at pH 7.4 for 3 days (Fig. 5), retaining at least 90% of the initial hydrogel mass. However, the peptide-crosslinked hydrogels were rapidly degraded by both collagenase and proteinase K, where the majority of the mass loss occurred in the first 5 hours (Fig. 5A). The peptoid-crosslinked hydrogels were likewise tested and were found to be markedly more stable under enzymatic conditions (Fig. 5B). For the peptoid-crosslinked hydrogels, no mass loss was detected over the 72 hour enzyme challenge with either proteinase K or collagenase. This innate proteolytic resistance renders this new hydrogel system particularly promising for longer term *in vitro* and *in vivo* experiments, where secreted proteases may be plentiful.

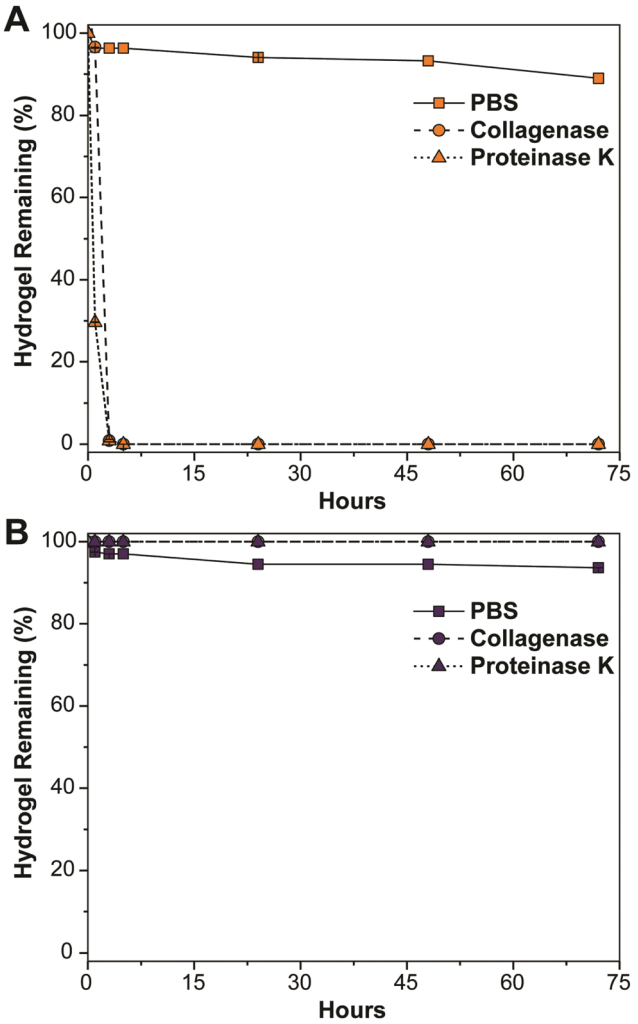

Fig. 5 (A) Stability of 10 wt% hydrogels crosslinked with a peptide control in phosphate buffered saline with and without the addition of collagenase (20 μg mL^{-1}, 255 units per mg) or proteinase K (20 μg mL^{-1}) over the course of 3 days. (B) Stability of 10 wt% hydrogels crosslinked with sequence **2** under the same conditions as part A.

Cytocompatibility of peptoid-crosslinked hydrogels

Previous reports have indicated minimal cytotoxicity of non-sequence specific peptoids toward multiple mammalian cell types, including human adipose-derived stem cells in thermally-gelled hydrogels,[26] human epithelial type 2 cells in culture with soluble peptoid polymers,[43] and human hepatoblastoma cells in culture with peptoid-based micelles.[44,45] Sequence-defined peptoid substrates, however, have been investigated both *in vitro* and *in vivo* for many biological applications, including helical mimics of antibacterial peptides.[46–48] Some of these sequences have exhibited cytotoxicity to mammalian cell types, such as normal human lung fibroblasts.[49] Therefore, to investigate the cytocompatibility of the helical peptoids crosslinked into a hydrogel platform here, we functionalized our hydrogels with a pendant cell adhesive peptide (GCGYGRGDSPG) by incorporating the peptide in the macromer solution (2 mM), which enabled reaction *via* photoinitiated thiol–ene chemistry during crosslinking (Fig. 6A). We subsequently cultured human dermal fibroblasts for 24 hours and allowed them to adhere to the hydrogels. Metabolic activity was assessed *via* MTT assay and found to be equivalent to dermal fibroblasts on both peptide-crosslinked hydrogels and tissue culture polystyrene controls (Fig. 6B). All of the hydrogels indicated high viabilities of approximately 100%, with the exception of the peptide-crosslinked hydrogels, which were slightly greater than 100% but within error. Furthermore, the attached cell spread areas were similar for cells on both the peptide and peptoid-crosslinked hydrogels (Fig. 6C), indicating similar elastic moduli between the two hydrogels. For reference, the human dermal fibroblasts were also cultured on glass, which is orders of magnitude stiffer than the hydrogels and subsequently showed much larger cell spread areas (Fig. S10, ESI†). To visualize the live cells, a LIVE/DEAD stain was applied to the dermal fibroblasts adhered to the surface of both peptide and peptoid-crosslinked hydrogels (Fig. 6D). Live cells appeared green, while dead cells appeared red. No dead cells were visible on the hydrogel surfaces by fluorescent microscopy, which may be due to detachment upon cell death. However, large numbers of living cells were visible for both hydrogel conditions, which supported the high viability indicated by the MTT assay results. Based off the microscopy images, a live cell density of approximately 4800 cells per cm^2 was observed on the peptoid-crosslinked

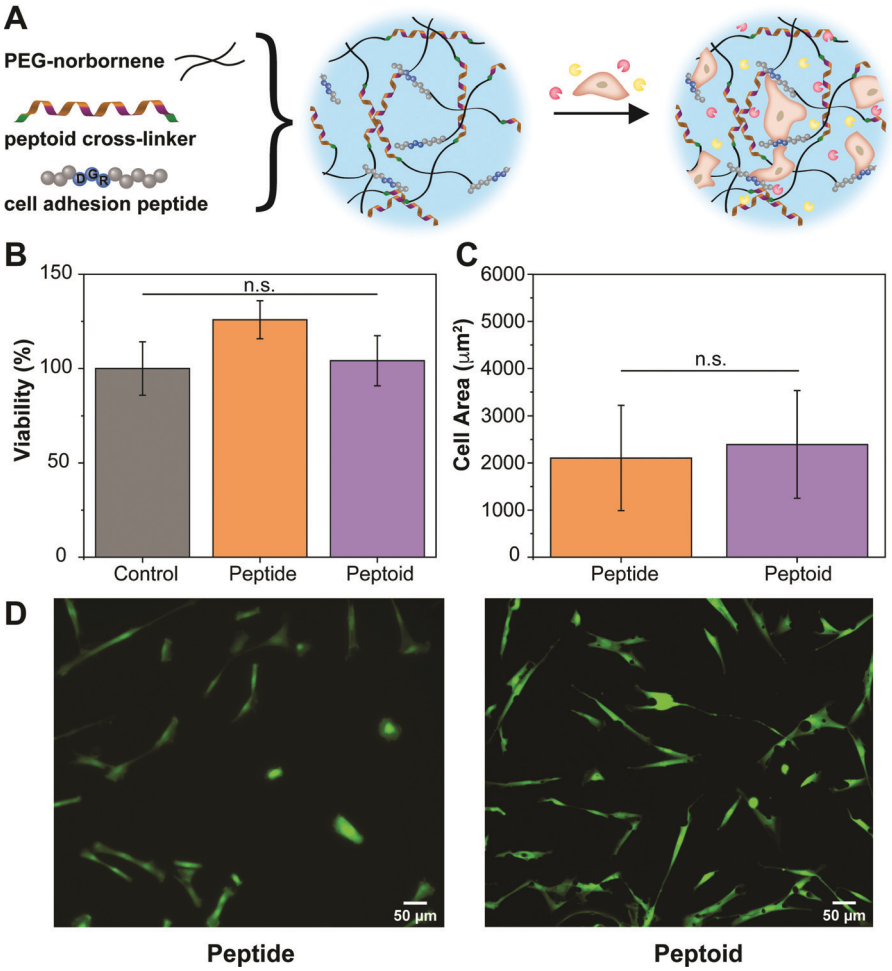

Fig. 6 (A) Schematic of hydrogel formation with the RGD-containing peptide for cell adhesion. Hydrogel schematic is a "top-down" view, as the cells were only seeded on top of the hydrogels. (B) Viability of dermal fibroblasts on a 5 wt% hydrogel crosslinked with sequence **2**, collected *via* MTT assay. (C) Average cell areas of dermal fibroblasts imaged on peptide and peptoid-crosslinked hydrogels. (D) Representative fluorescent microscopy images of dermal fibroblasts adhered to the peptide and peptoid-crosslinked hydrogels. Live cells appear green due to calcein-AM cleavage.

hydrogels, which compared favorably with the cell density on peptide-crosslinked hydrogels and glass (Fig. S11, ESI†).

Conclusions

Hierarchical control over monomer sequence and chain shape confers tightly integrated biochemical and biophysical properties in the native extracellular matrix. Recapitulating this hierarchical control with synthetic molecules in engineered ECM mimics may provide an extra handle with which to fine tune matrix properties and decouple parameters such as structure, network connectivity, mechanics, and bioactivity. Here, we developed the use of sequence-defined, helical peptoids as crosslinkers in a PEG hydrogel fabricated *via* photoinitiated thiol–ene chemistry. Peptoid structure was found to increase matrix stiffness with longer chain lengths, indicating an avenue to control bulk properties with peptoid monomer sequence and chain shape in a fashion similar to peptide crosslinkers. Uniquely, the *N*-substituted backbone of the peptoids conferred high stability to the hydrogels and resistance to proteolysis. The value and potential utility of this platform was demonstrated by incorporation of a cell adhesion peptide and culture of human dermal fibroblasts. This work provides a step toward the control of matrix properties with abiotic monomer sequences and the development of hierarchical, synthetic ECM with long term stability for applications in tissue engineering and *in vitro* disease models.

Conflicts of interest

There are no conflicts to declare.

Acknowledgements

We thank Roshan Chandrashekar for assistance with preliminary data collection. This research was supported by the Burroughs Wellcome Fund (CASI-1015895, A. M. R.) and by the National Science Foundation (NSF MRSEC DMR-1720595 A. M. R.). In addition, M. J. A. was supported through a National Science Foundation Graduate Research Fellowship (Program Award No. 000392968). The authors acknowledge the use of shared research facilities supported in part by the Texas Materials Institute, the

Center for Dynamics and Control of Materials: an NSF MRSEC (DMR-1720595), and the NSF National Nanotechnology Coordinated Infrastructure (ECCS-1542159). We also acknowledge the use of shared facilities in the Targeted Therapeutic Drug Discovery & Development Program (CPRIT Core Facilities Support Award (grant # RP160657)) and the UT Proteomics Facility.

References

1 K. Medini, B. W. Mansel, M. A. K. Williams, M. A. Brimble, D. E. Williams and J. A. Gerrard, *Acta Biomater.*, 2016, **43**, 30–37.
2 L. J. Dooling and D. A. Tirrell, *ACS Cent. Sci.*, 2016, **2**, 812–819.
3 J. Patterson, M. M. Martino and J. A. Hubbell, *Mater. Today*, 2010, **13**, 14–22.
4 J. Zhu, *Biomaterials*, 2010, **31**, 4639–4656.
5 C. R. Nuttelman, M. C. Tripodi and K. S. Anseth, *Matrix Biol.*, 2005, **24**, 208–218.
6 D. L. Hern and J. A. Hubbell, *J. Biomed. Mater. Res.*, 1997, **39**, 266–276.
7 R. H. Schmedlen, K. S. Masters and J. L. West, *Biomaterials*, 2002, **23**, 4325–4332.
8 J. A. Rowley, G. Madlambayan and D. J. Mooney, *Biomaterials*, 1999, **20**, 45–53.
9 A. M. Hilderbrand, E. M. Ford, C. Guo, J. D. Sloppy and A. M. Kloxin, *Biomater. Sci.*, 2020, **8**, 1256–1269.
10 M. J. Austin and A. M. Rosales, *Biomater. Sci.*, 2019, **7**, 490–505.
11 M. A. Washington, S. C. Balmert, M. V. Fedorchak, S. R. Little, S. C. Watkins and T. Y. Meyer, *Acta Biomater.*, 2018, **65**, 259–271.
12 S. Motamed, M. P. Del Borgo, K. Kulkarni, N. Habila, K. Zhou, P. Perlmutter, J. S. Forsythe and M. I. Aguilar, *Soft Matter*, 2016, **12**, 2243–2246.
13 S. Motamed, M. P. Del Borgo, K. Zhou, K. Kulkarni, P. J. Crack, T. D. Merson, M. I. Aguilar, D. I. Finkelstein and J. S. Forsythe, *Front. Bioeng. Biotechnol.*, 2019, **7**, 1–12.
14 S. M. Miller, R. J. Simon, S. Ng, R. N. Zuckermann, J. M. Kerr and W. H. Moos, *Bioorg. Med. Chem. Lett.*, 1994, **4**, 2657–2662.
15 K. Kirshenbaum, A. E. Barron, R. A. Goldsmith, P. Armand, E. K. Bradley, K. T. V. Truong, K. A. Dill, F. E. Cohen and R. N. Zuckermann, *Proc. Natl. Acad. Sci. U. S. A.*, 1998, **95**, 4303–4308.
16 R. N. Zuckermann, J. M. Kerr, W. H. Moosf and S. B. H. Kent, *J. Am. Chem. Soc.*, 1992, **114**, 10646–10647.
17 L. Guo, J. Li, Z. Brown, K. Ghale and D. Zhang, *Biopolymers*, 2011, **96**, 596–603.
18 L. Guo, S. H. Lahasky, K. Ghale and D. Zhang, *J. Am. Chem. Soc.*, 2012, **134**, 9163–9171.
19 C. Fetsch, A. Grossmann, L. Holz, J. F. Nawroth and R. Luxenhofer, *Macromolecules*, 2011, **44**, 6746–6758.
20 C. W. Wu, T. J. Sanborn, K. Huang, R. N. Zuckermann and A. E. Barron, *J. Am. Chem. Soc.*, 2001, **123**, 6778–6784.
21 C. W. Wu, T. J. Sanborn, R. N. Zuckermann and A. E. Barron, *J. Am. Chem. Soc.*, 2001, **123**, 2958–2963.
22 B. C. Lee, R. N. Zuckermann and K. A. Dill, *J. Am. Chem. Soc.*, 2005, **127**, 10999–11009.
23 K. T. Nam, S. A. Shelby, P. H. Choi, A. B. Marciel, R. Chen, L. Tan, T. K. Chu, R. A. Mesch, B. C. Lee, M. D. Connolly, C. Kisielowski and R. N. Zuckermann, *Nat. Mater.*, 2010, **9**, 454–460.
24 H. P. R. Mangunuru, H. Yang and G. Wang, *Chem. Commun.*, 2013, **49**, 4489–4491.
25 Z. Wu, M. Tan, X. Chen, Z. Yang and L. Wang, *Nanoscale*, 2012, **4**, 3644–3646.
26 S. Xuan, C. U. Lee, C. Chen, A. B. Doyle, Y. Zhang, L. Guo, V. T. John, D. Hayes and D. Zhang, *Chem. Mater.*, 2016, **28**, 727–737.
27 K. H. A. Lau, *Biomater. Sci.*, 2014, **2**, 627–633.
28 T. J. Sanborn, C. W. Wu, R. N. Zuckermann and A. E. Barron, *Biopolymers*, 2002, **63**, 12–20.
29 A. M. Rosales, H. K. Murnen, S. R. Kline, R. N. Zuckermann and R. A. Segalman, *Soft Matter*, 2012, **8**, 3673–3680.
30 H. K. Murnen, A. M. Rosales, A. V. Dobrynin, R. N. Zuckermann and R. A. Segalman, *Soft Matter*, 2013, **9**, 90–98.
31 A. M. Oelker, S. M. Morey, L. G. Griffith and P. T. Hammond, *Soft Matter*, 2012, **8**, 10887–10895.
32 H. He, M. Sofman, A. J.-S. Wang, C. C. Ahrens, W. Wang, L. G. Griffith and P. T. Hammond, *Biomacromolecules*, 2020, **21**, 566–580.
33 A. A. Aimetti, A. J. Machen and K. S. Anseth, *Biomaterials*, 2009, **30**, 6048–6054.
34 S. B. Anderson, C.-C. Lin, D. V. Kuntzler and K. S. Anseth, *Biomaterials*, 2011, **32**, 3564–3574.
35 J. L. Leight, D. L. Alge, A. J. Maier and K. S. Anseth, *Biomaterials*, 2013, **34**, 7344–7352.
36 K. M. Schultz, K. A. Kyburz and K. S. Anseth, *Proc. Natl. Acad. Sci. U. S. A.*, 2015, **112**, E3757–E3764.
37 B. D. Fairbanks, M. P. Schwartz, A. E. Halevi, C. R. Nuttelman, C. N. Bowman and K. S. Anseth, *Adv. Mater.*, 2009, **21**, 5005–5010.
38 L. A. Sawicki and A. M. Kloxin, *Biomater. Sci.*, 2014, **2**, 1612–1626.
39 M. Rzeigui, M. Traikia, L. Jouffret, A. Kriznik, J. Khiari, O. Roy and C. Taillefumier, *J. Org. Chem.*, 2020, **85**, 2190–2201.
40 H.-M. Shin, C.-M. Kang, M.-H. Yoon and J. Seo, *Chem. Commun.*, 2014, **50**, 4465–4468.
41 J. R. Stringer, J. A. Crapster, I. A. Guzei and H. E. Blackwell, *J. Am. Chem. Soc.*, 2011, **133**, 15559–15567.
42 C. C. Ahrens, M. E. Welch, L. G. Griffith and P. T. Hammond, *Biomacromolecules*, 2015, **16**, 3774–3783.
43 S. Xuan, S. Gupta, X. Li, M. Bleuel, G. J. Schneider and D. Zhang, *Biomacromolecules*, 2017, **18**, 951–964.
44 A. Li and D. Zhang, *Biomacromolecules*, 2016, **17**, 852–861.
45 C. Fetsch, S. Flecks, D. Gieseler, C. Marschelk, J. Ulbricht, K. H. Van Pée and R. Luxenhofer, *Macromol. Chem. Phys.*, 2015, **216**, 547–560.
46 A. M. Czyzewski, H. Jenssen, C. D. Fjell, M. Waldbrook, N. P. Chongsiriwatana, E. Yuen, R. E. W. Hancock and A. E. Barron, *PLoS One*, 2016, **11**, e0135961.
47 N. P. Chongsiriwatana, J. A. Patch, A. M. Czyzewski, M. T. Dohm, A. Ivankin, D. Gidalevitz, R. N. Zuckermann and A. E. Barron, *Proc. Natl. Acad. Sci. U. S. A.*, 2008, **105**, 2794–2799.
48 N. P. Chongsiriwatana, M. Wetzler and A. E. Barron, *Antimicrob. Agents Chemother.*, 2011, **55**, 5399–5402.
49 J. Lee, D. Kang, J. Choi, W. Huang, M. Wadman, A. E. Barron and J. Seo, *Bioorg. Med. Chem. Lett.*, 2018, **28**, 170–173.